J Sol-Gel Sci Technol (2015) 76:289–297
DOI 10.1007/s10971-015-3776-3

ORIGINAL PAPER

Room-temperature multiferroic properties of $0.6BiFeO_3$–$0.4(Bi_{0.5}Na_{0.5})_{(1-x)}Ba_xTiO_3$ solid-solution ceramics

C. M. Zhu[1] · L. G. Wang[1] · S. L. Yuan[1] · Z. M. Tian[1]

Received: 16 March 2015 / Accepted: 18 June 2015 / Published online: 26 June 2015

Abstract The $0.6BiFeO_3$–$0.4(Bi_{0.5}Na_{0.5})_{(1-x)}Ba_xTiO_3$ (short for BF-$BN_{(1-x)}Ba_xT$) ($x = 0$, 0.2, 0.3, 0.4, 0.5) solid-solution ceramics were fabricated by a sol–gel method. The presence of constituent phases in ceramics was investigated by X-ray diffraction. It indicates that all of the samples are single phase. Not only that, it also proves the rhombohedral structure of the samples. Multiferroic properties dependent on the doping content of Ba ions were studied systematically. The ferroelectricity and ferromagnetism were tested, displaying the maximum values of remnant polarization and remnant magnetization at $x = 0.4$ simultaneously. With the increasing in x, the peak of dielectric constant depending on temperature shifts toward to the lower temperature range. In addition, the dielectric diffuse degree also increases monotonically as x increases to 0.5.

Graphical Abstract (a–e) Magnetization hysteresis loops of BF-$BN_{(1-x)}Ba_xT$ ($x = 0$, 0.2, 0.3, 0.4, 0.5) solid solutions at room temperature and (f) the evolutions of M_r and H_c with x.

✉ S. L. Yuan
yuansl@hust.edu.cn

✉ Z. M. Tian
tianzhaoming@hust.edu.cn

[1] School of Physics, Huazhong University of Science and Technology, Wuhan 430074, People's Republic of China

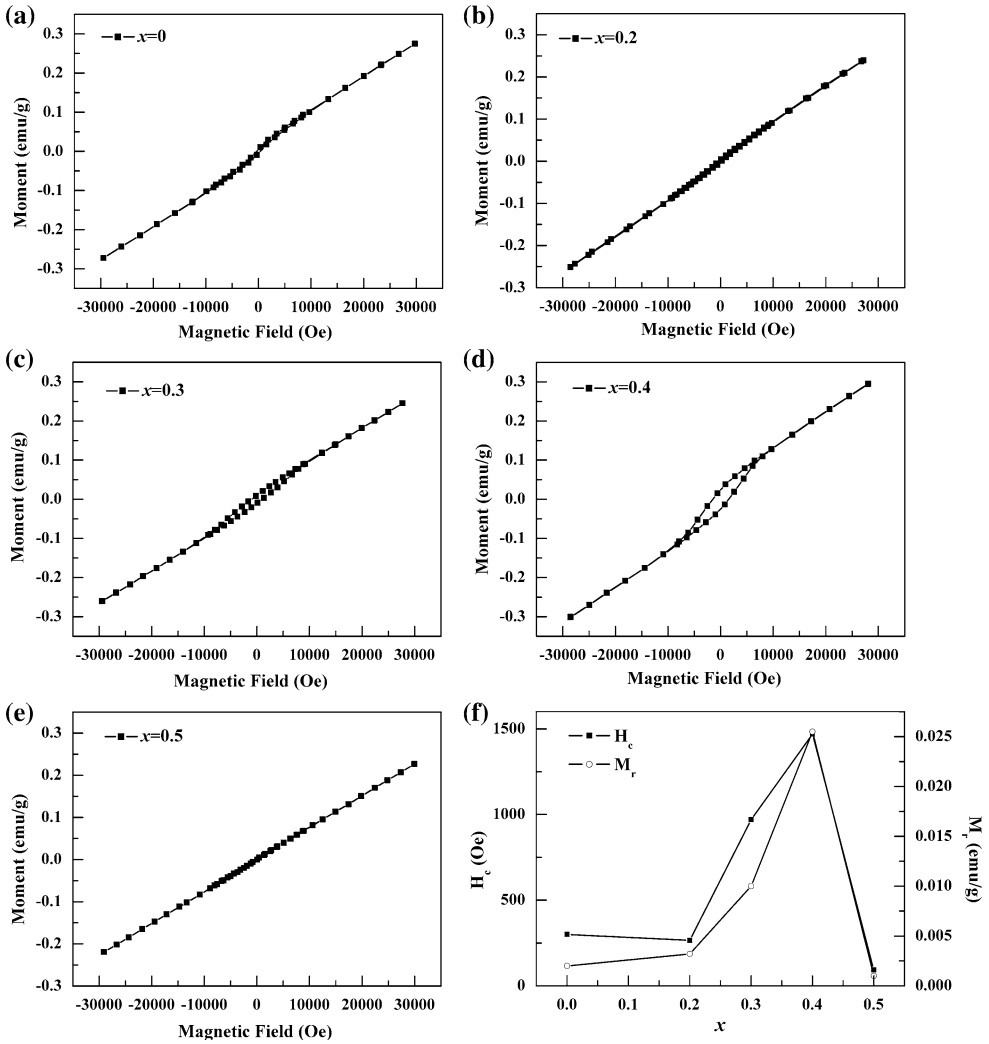

Keywords Sol–gel processes · Dielectric properties · Magnetic properties · Multiferroics

1 Introduction

We believe that multiferroic materials [1–3] that exhibit ferroelectric and ferromagnetic properties simultaneously have attracted increasing interest for a long period of time. The potential application in fundamental physics even multifunctional devices such as storage media, spintronic devices and sensors should just be the very reason [4]. However, the single-phase multiferroics in nature are very few because of the coexistence with ferroelectricity and ferromagnetism, which requires empty and partially filled transition metal orbital, respectively [5].

$BiFeO_3$ (BF) is a rare single-phase multiferroic material characterized by the high ferroelectric Curie temperature T_C ($T_C \sim 1103$ K) and antiferromagnetic Néel temperature T_N ($T_N \sim 643$ K) [6]. The ferroelectricity of BF comes from Bi ions $6s^2$ lone-pair electrons while the magnetism is originated from the partially filled *d*-orbitals of Fe. Unfortunately, the relative high leakage current and unwanted secondary phases become the key factors for hindering the research of BF [7, 8]. To stabilize the perovskite phase and enhance the electric, magnetic and magnetoelectric properties of BF, doping other elements, such as La or Mn [9], and even many other ABO_3 perovskite phases such as $PbTiO_3$ [10], $Na_{0.5}K_{0.5}NbO_3$ [11] and $SrTiO_3$ [12], is used to form solid solutions with BF. Among these, $Bi_{0.5}Na_{0.5}TiO_3$ (BNT) is a lead-free rhombohedral perovskite-type ferroelectric materials with $T_C = 320$ °C [13]. Improvement in ferroelectric and magnetic properties of BF-BNT has been reported in comparison with BF [14]. In order to obtain better properties, further works are ongoing.

In this paper, BF-$BN_{(1-x)}Ba_xT$ ($x = 0$, 0.2, 0.3, 0.4, 0.5) ceramics were synthesized by a sol–gel technique. The reason for choosing this composite is based on the interesting observations of approved multiferroic properties in BF solid solutions with $BaTiO_3$ [15] and $Bi_{0.5}Na_{0.5}TiO_3$ [16]. Also, to our knowledge, the size of Ba ions (0.135 nm) is quite larger than Bi ions (0.103 nm), so doping Ba ions in BF-BNT may cause some structural distortion, and therefore, the properties will be changed in comparison with BF-BNT.

2 Experimental procedure

The BF-$BN_{(1-x)}Ba_xT$ ($x = 0$, 0.2, 0.3, 0.4, 0.5) ceramics were fabricated by a sol–gel method [16]. At first, raw materials of 99.9 % purity $Bi(NO_3)_3{\cdot}5H_2O$, $Fe(NO_3)_3{\cdot}9H_2O$, $NaNO_3$, $BaCO_3$, butyl titanate and citric acid were dissolved in distilled water. In this process, citric acid and metal cations have a molar ratio of 1.5:1. The detailed values are listed in Table 1. Then, the solution was maintained at room temperature under strong magnetic stirring for 2 h. After that, the pH value of mix solution was adjusted to 7–8 by adding ammonia. About 15 h was still needed to thoroughly homogenize the solution to form sol. Afterward, the sol was heated in water bath and kept the temperature 373 K for 5 h to form gel. The gel was dried in oven at 403 K for 5 h and then ground and calcined at 773 K to form the precursor powers. Finally, the powders were ground in an agate bowl for about 2 h and then pressed into disks with 10 mm in diameter and 1 mm in thickness. In our experiments, the disks were sintered at 1223 K for 6 h. To measure the electrical properties, electrodes with silver paste were applied to both surfaces.

Crystal structures were investigated by a Philips Panalytical X'pert diffractometer (XRD) using the iron-filtered Cu-Kα radiation ($\lambda = 0.15406$ nm) in the 2θ range of 20°–80° with a step size of 0.02 °. Magnetic measurements were taken using a commercial Physical Property Measurement System (PPMS, Quantum Design) with the apparatus error of 0.5 %. The polarization hysteresis loops at room temperature were measured by a commercial FE test system (PremierII, Radiant Technologies). The dielectric properties of the ceramics were obtained with a precision impedance analyzer (PST-2000H) with an ac voltage of 1 V, and the error of apparatus is 0.05 %.

3 Results and discussion

XRD patterns of the investigated ceramics ($x = 0$, 0.2, 0.3, 0.4, 0.5) are plotted in Fig. 1a. All the diffraction peaks are well matched with the structure of BF-$BN_{(1-x)}Ba_xT$, which is identified as pure phase without any other observable impurity (e.g., $Bi_2Fe_4O_9$, Bi_2O_3 and Fe_2O_3). All the samples of BF-$BN_{(1-x)}Ba_xT$ are rhombohedral perovskite structure compared with the PDF card numbered 01-072-2035, and it also indicates that the pure-phase BF-$BN_{(1-x)}Ba_xT$ can be synthesized by sol–gel method. In order to give a more explicit picture, a magnified diffraction patterns at the vicinity of $2\theta = 22$–23° can be seen in Fig. 1b. With the increasing content of Ba ions, the peak of (100) shifts toward to lower angles indicating the increase in lattice parameter. The dependence of lattice parameter (d) on the doping content (x) is depicted in the inset of Fig. 1b. Increasing with the doping composition, lattice parameter increases monotonously, which is consistent with the theoretical value calculated by Braggs formula. It can be understood that when Ba ions are added to BF-BNT, the higher size of Ba ions results in the increase in effective ionic radius of A site. The higher amount of Ba ions will slightly distort the unit cell and induce strain in the lattice, which can lead to an increase in lattice parameter and even result in the shift of diffraction peak, ultimately. This might be important for the multiferroic properties at room temperature of the compound.

The ferroelectric properties have been evaluated through measuring the room-temperature polarization–electric field (P–E) hysteresis loops with 10 Hz. It is a most important character to study the ferroelectric behavior. The P–E loops with different contents of Ba ions are plotted in Fig. 2. Ferroelectric behavior is observed in the all samples. Firstly, keeping frequency stable, P_r increases gradually with an increase in electric field owing to larger electric field providing higher level of driving power, which is responsible for the ferroelectric domains reversal. Therefore, higher driving power enhances the volume of ferroelectric domains even the total ferroelectric polarization

Table 1 Quantity of the reagents with different values of x

Reagents (g) x	$Bi(NO_3)_3{\cdot}5H_2O$	$Fe(NO_3)_3{\cdot}9H_2O$	$NaNO_3$	Butyl titanate	$BaCO_3$	Citric acid
0	3.8805	2.424	0.17	1.3614	–	6.3042
0.2	3.6865	2.424	0.136	1.3614	0.1579	6.3042
0.3	3.5895	2.424	0.119	1.3614	0.2368	6.3042
0.4	3.4925	2.424	0.102	1.3614	0.3157	6.3042
0.5	3.3955	2.424	0.085	1.3614	0.3947	6.3042

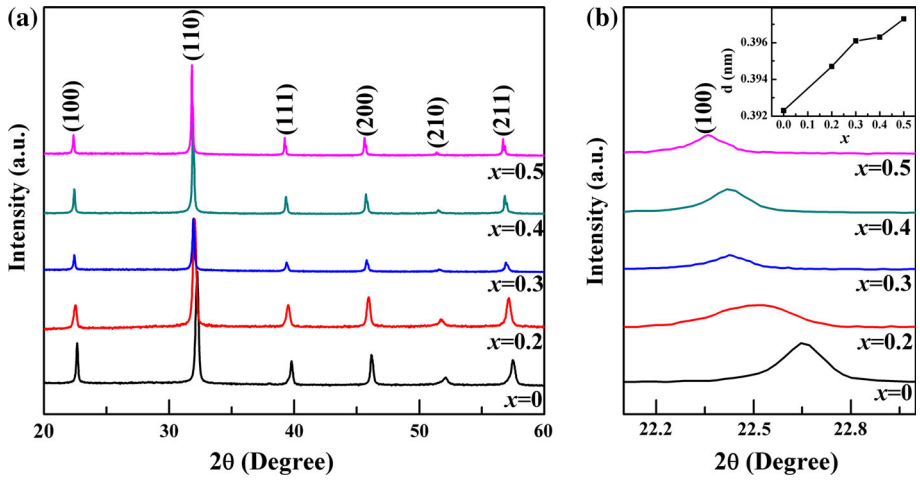

Fig. 1 **a** XRD patterns of BF-$BN_{(1-x)}Ba_xT$ ($x = 0$, 0.2, 0.3, 0.4, 0.5) solid solutions, **b** magnified patterns of peak (100) and the *inset* shows the evolutions of lattice parameter with x

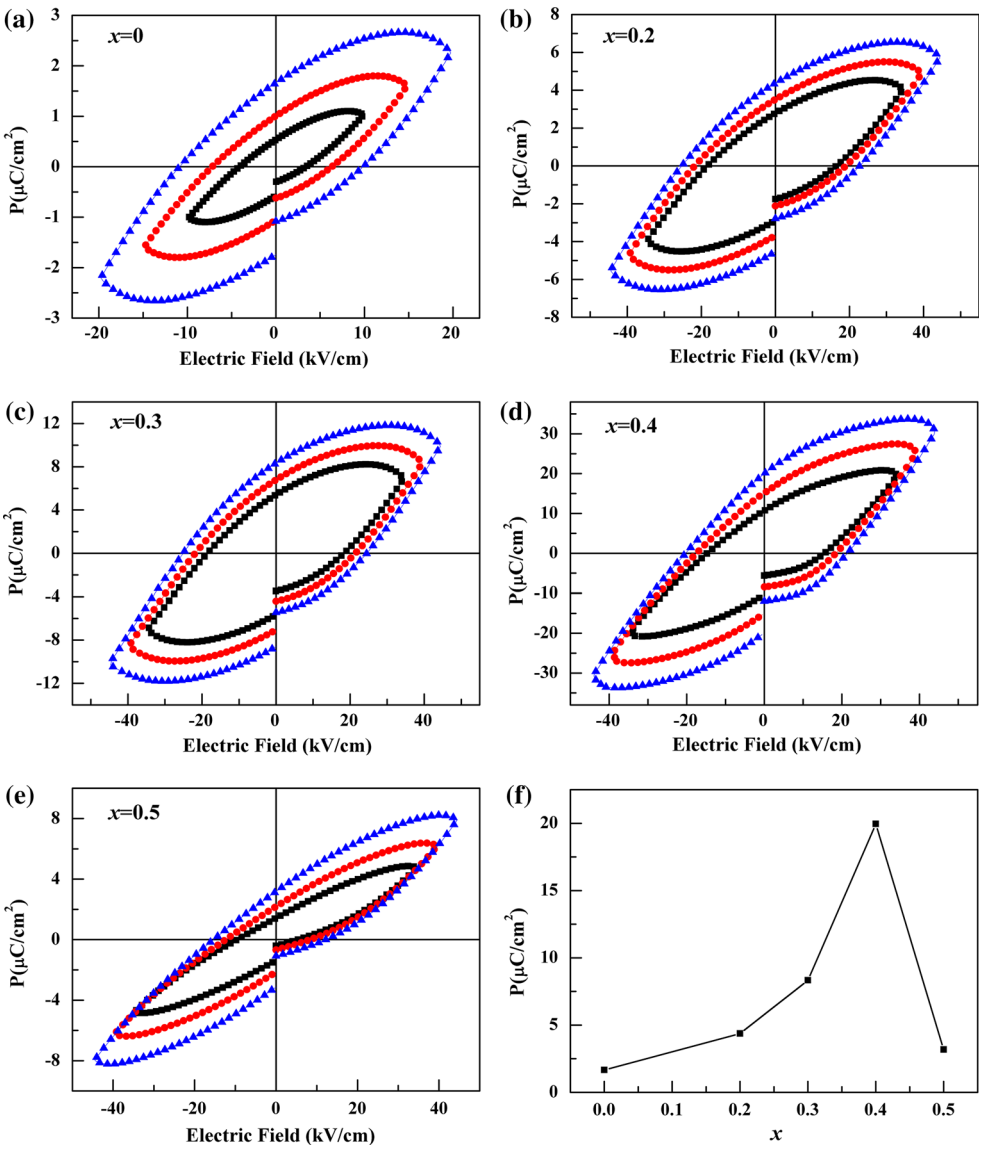

Fig. 2 **a–e** Polarization hysteresis loops of BF-$BN_{(1-x)}Ba_xT$ ($x = 0$, 0.2, 0.3, 0.4, 0.5) solid solutions at room temperature and **f** the evolutions of P_r with x

including the parameters such as E_c and P_r. Here, E_c is the coercive electric field and P_r is the remnant polarization. During measurement, the samples are polarized with applied field. When applied electric field is turn off, the polarization is not zero and it is named P_r. When electric field is applied again and make the polarization zero, the value of electric field is E_c. Then, as shown in Fig. 2a, just low-field *P–E* loops are observed for BF-BNT without Ba ions. Higher field is restricted because of the great electric leakage, which also results in the unsaturated *P–E* loops. For the other samples, clear *P–E* loops with higher applied electric field can be detected. Although all the samples do not show saturated *P–E* loops, which agree well with the previous reports on BF solid-solution systems [17–19], the ferroelectric properties of our samples are much improved in comparison with those of BF-BNT. Compared with Fig. 2a, as the doping content of Ba ions increases, E_c and P_r increase from $E_c = 9.8$ kV/cm and $P_r = 1.66$ μC/cm^2 for $x = 0$ to $E_c = 21.4$ kV/cm and $P_r = 19.95$ μC/cm^2 for $x = 0.4$. E_c and P_r roughly increase accompanied with the Ba ions increasing. Figure 2f also shows the evolutions of P_r with the content of Ba. The unsaturated *P–E* loops may arise from leakage current shown in Fig. 3 and the partial reversal of the polarization. To our knowledge, oxygen vacancies that can be formed in BF-BNT lattice lead to pinning of the domain wall and trapping of charge carriers; thus, it could increase the leakage current [20]. As a result, the improvement in ferroelectric properties should be attributed to the suppressing of oxygen vacancy and the weakening of the defect mobility, which can make a contribution to domain pinning [20]. When Ba ions increase from 0.4 to 0.5, the *P–E* hysteresis curves appear very leaky and the P_r presents a sharp decrease with the *P–E* loops displaying more open loops at 0.5. Porosity, grain boundary, grain size and crystal defects are important factors that can affect the ferroelectric behavior. Sample with $x = 0.5$ has a bigger lattice constant, which can be accompanied with the formation of higher porosity. Larger number of insulating grain boundaries and more grain–grain interface

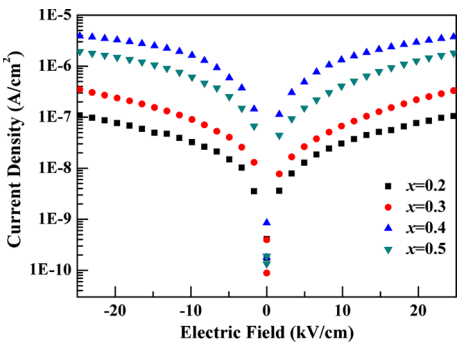

Fig. 3 Leakage current versus electric field curves of BF-$BN_{(1-x)}Ba_xT$ ($x = 0.2$, 0.3, 0.4, 0.5) solid solutions

space can act as a barrier for electric current, resulting in the anomalous behavior in sample of $x = 0.5$. In brief, evidenced by the XRD patterns in Fig. 1, the changed ferroelectric polarization can be attributed to the distortion of BF-$BN_{(1-x)}Ba_xT$ with doping of Ba ions. The introduction of Ba ions breaks the original order of BF-BNT structure inducing structural distortion and changing the oxygen vacancy. In addition, the Ba ions may be formed to $BaTiO_3$ and then influence the ferroelectric properties of BF-$BN_{(1-x)}Ba_xT$ ceramics, which is similar to the previous studies [21–23].

Figure 4 shows the variation of dielectric constant (ε_r) as a function of temperature for different frequencies (10, 100, 500 kHz and 1 MHz). For the samples, dielectric constants increase at low temperature followed by the appearance of peaks at the range of 300–400 °C, which is at the vicinity of ferroelectric–paraelectric transition temperature of BNT and the antiferromagnetic Néel temperature of BF. What is more, the peak position shifts toward to lower temperature side as x increases. As we all know, the ferroelectric–paraelectric transition temperature of $BaTiO_3$ is around its Curie temperature ($T_C = 120$ °C) [24] and that of BNT and BF is $T_C = 320$ °C [25] and 830 °C, respectively. The ferroelectric–paraelectric transition temperature of $BaTiO_3$ is lower than that of BNT and BF. Therefore, that may be the reason of the shift toward to low temperature. Another reason may be related to the magnetoelectric coupling. The antiferromagnetic Néel temperature of BF is 370 °C. The magnetic structure of BF is of G type with each Fe^{3+} magnetic ion surrounded by six Fe^{3+} nearest neighbors with antiparallel magnetic moments. Doping with different ions can induce changes of cation displacements, alterations of tilt angle, distortion, strain of oxygen octahedral and even the canting of the spiral spin modulation due to a structural distortion. In our samples, the content of Ba ions may induce the spiral spin structural distortion of BF. So, the peaks shifting toward to the lower temperature with increasing of Ba can be related to the change of magnetic ordering in BF. As an effect of vanishing magnetic order on electric order, Landau–Devonshire theory of phase transitions has predicated this type of dielectric anomaly in the magnetoelectrically ordered systems [26]. It is consistent with the manipulation of magnetoelectric interaction, which can induce the shift in magnetic transition temperature due to an electric field. Of course, further investigation is still needed to reveal the real physical natures of the dielectric anomaly in BF-$BN_{(1-x)}Ba_xT$. As shown in Fig. 4, another phenomenon is that the dielectric peaks broaden with x increasing. The results should imply that diffuse phase transition exists in the samples and that it is enhanced with increasing content of Ba ions. These are in good agreement with other reports about Ba doping [27].

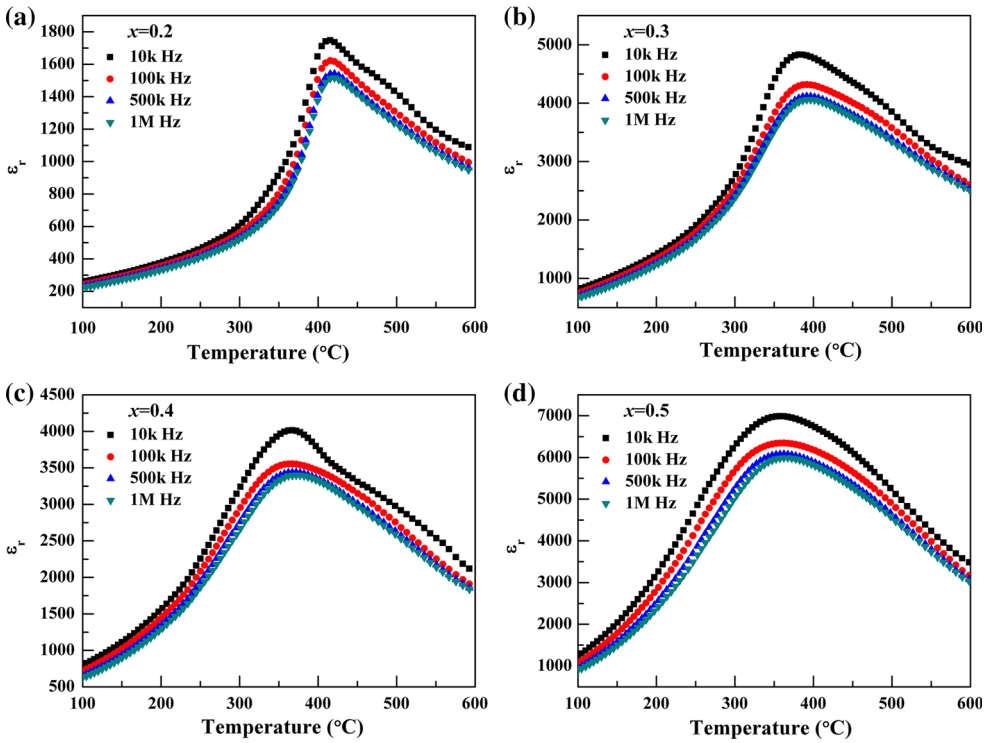

Fig. 4 Temperature dependence of dielectric constant for BF-$BN_{(1-x)}Ba_xT$ ($x = 0.2, 0.3, 0.4, 0.5$) solid solutions at different frequencies (10, 100, 500 kHz and 1 MHz)

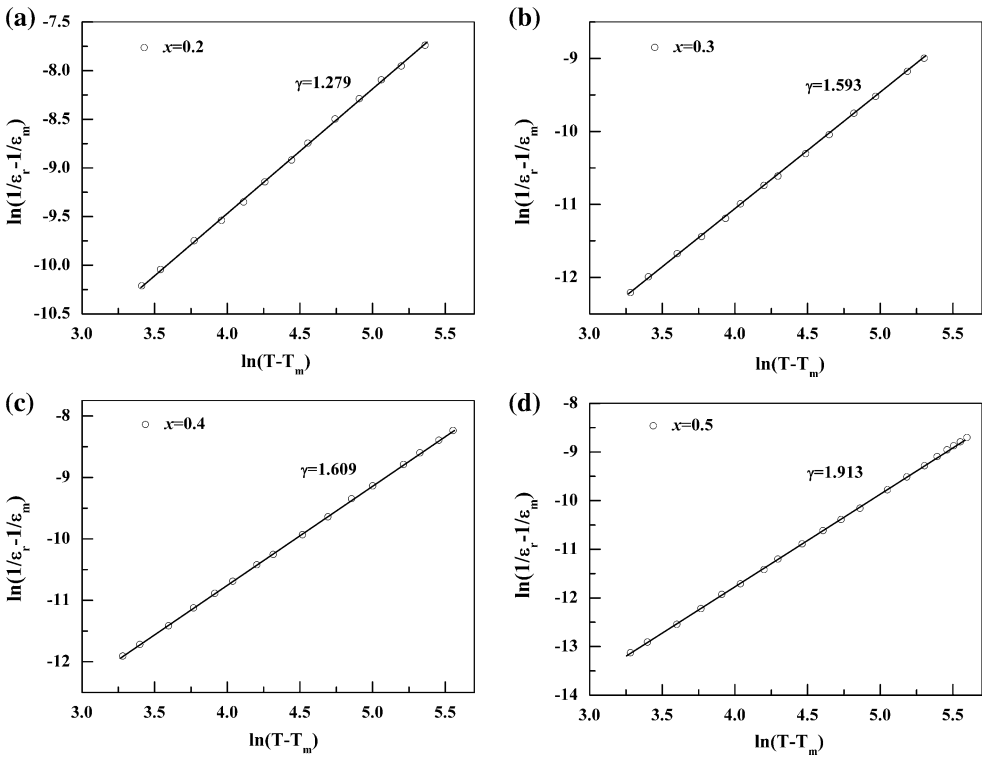

Fig. 5 Variation of $\ln(1/\varepsilon_r - 1/\varepsilon_m)$ with $\ln(T - T_m)$ for BF-$BN_{(1-x)}Ba_xT$ ($x = 0.2$, 0.3, 0.4, 0.5) at 10 kHz

In order to further characterize the dielectric dispersion and diffuseness of the phase transition, a modified Curie–Weiss law proposed by Uchino and Nomura [28] is employed: $1/\varepsilon_r - 1/\varepsilon_m = A(T - T_m)^{\gamma}$, where ε_m is the maximum value of the dielectric constant at the phase transition temperature T_m, γ is the degree of diffuseness, and A is a constant. The value of γ in normal ferroelectric is 1, and the ideal relaxor ferroelectric is 2. Figure 5 plots the

variation of $\ln(1/\varepsilon_r - 1/\varepsilon_m)$ as a function of $\ln(T-T_m)$ at 10 k Hz for the BF-$BN_{(1-x)}Ba_xT$ ceramics. From the results, we can find that the values of γ are between 1 and 2, which proves that our samples indeed have the relaxor behavior as presented in Fig. 4. In addition, the values show a monotonic increasing as the x increases. It means that the diffuse degree of BF-$BN_{(1-x)}Ba_xT$ ceramics is increased by doping Ba ions. This case can be ascribed to the different ions occupied the equivalent site in crystal lattice randomly, and therefore, different components in crystal lattice can result in different phase transition temperatures and different breadths of transition temperature range.

In addition, temperature dependence of dielectric loss (tan δ) with various frequencies is plotted in Fig. 6. Dielectric loss is the energy dissipation through the dielectric system, and it is proportional to the imaginary part of the dielectric constant. During the range of low temperature, the value of dielectric loss is about 0.3 and is negligibly small. At higher temperature, value of dielectric loss increases sharply with a rise of temperature for all the samples because that charge carriers can gain a higher level of energy resulting in the increase in conductivity. What is also needed to pointed out is that the value of dielectric loss is small enough at room temperature and has a decreasing tendency as the content of Ba increases, which signifies the enhancement of some multiferroic properties and also helps the BF-$BN_{(1-x)}Ba_xT$ composite to be a very useful role for multifunctional application much further.

For investigating the different magnetic properties between $x = 0$ and the other samples, magnetization hysteresis (M–H) loops of the BF-$BN_{(1-x)}Ba_xT$ ($x = 0$, 0.2, 0.3, 0.4, 0.5) have been measured at 300 K with a maximum magnetic field of 30,000 Oe. Figure 7a–e displays the magnetic loops with nonzero remnant magnetization (M_r) of the samples, which reflects the presence of ferromagnetism at room temperature. In addition, M_r and coercive field (H_c) increase and then reduce in the order $x = 0$–0.4 and $x > 0.4$ as shown in Fig. 7f. It is worth mentioning that the optimal ferromagnetic behavior is observed at $x = 0.4$ with corresponding coercive field $H_c = 1500$ Oe and $M_r = 0.025$ emu/g, which is consistent with the degree of lattice deformation. The destruction of spiral spin structure can have an influence on the magnetic properties of the multiferroics. The Ba ions with large radius breaking the spiral spin structure of BF lead to the appearance of ferromagnetic characteristic. The decrease in H_c and M_r with $x = 0.5$ should be related to the overmuch content of Ba ions. It is likely that excessive structural distortion for space-modulated spiral spin structure decreases the magnetic properties. Of course, the magnetic properties are still considerably enhanced when Ba ions are induced. In comparison with the above results in Fig. 2, we can also conclude that there is a coexistence of ferroelectric and ferromagnetic properties among these ceramics at room temperature.

Eventually, although the patterns in Fig. 1 have proved the samples pure, it is necessary to exclude the properties

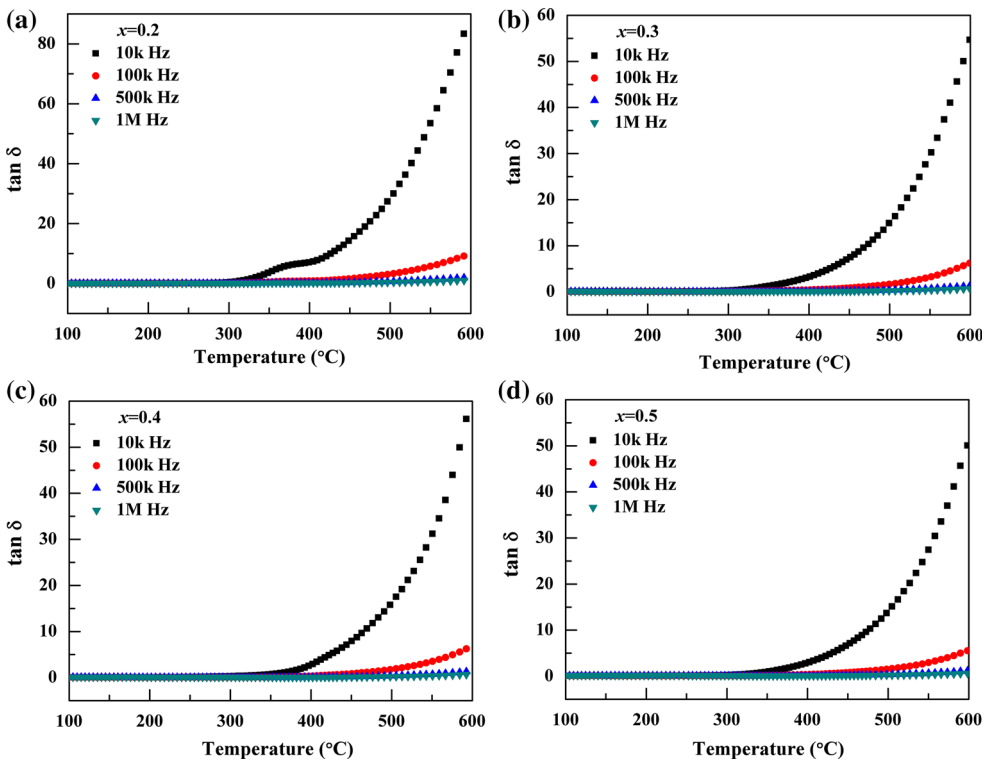

Fig. 6 Temperature dependence of dielectric loss for BF-$BN_{(1-x)}Ba_xT$ ($x = 0.2$, 0.3, 0.4, 0.5) solid solutions at different frequencies (10, 100, 500 kHz and 1 MHz)

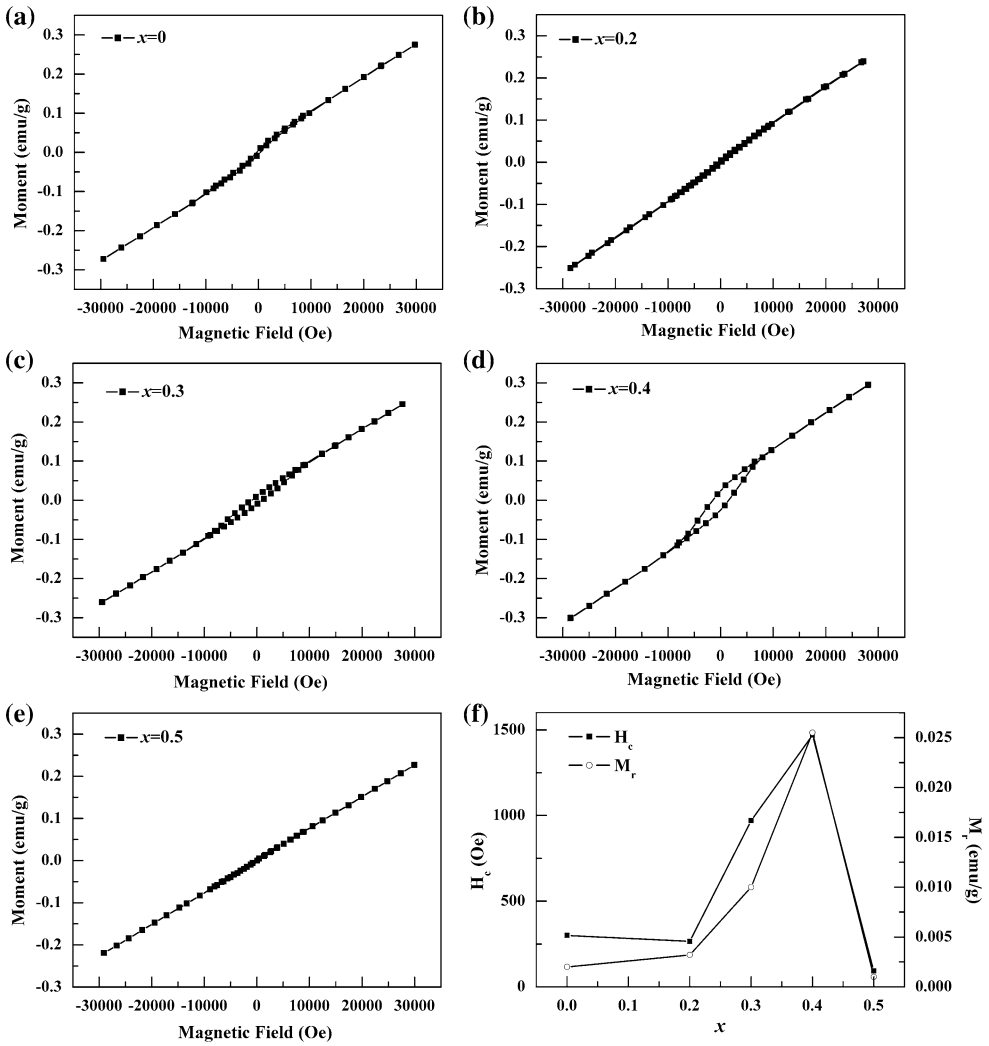

Fig. 7 **a–e** Magnetization hysteresis loops of BF-$BN_{(1-x)}Ba_xT$ ($x = 0$, 0.2, 0.3, 0.4, 0.5) solid solutions at room temperature and **f** the evolutions of M_r and H_c with x

contributed from the potential impurity phases such as Fe_2O_3, $Bi_2Fe_4O_9$ and $Bi_{25}FeO_{40}$ before ascribing the observed ferromagnetism to be intrinsic. At first, the BF-$BN_{(1-x)}Ba_xT$ has a larger H_c ($\sim$1 kOe) than Fe_2O_3 (<100 Oe), which exclude the possible origination from Fe_2O_3 impurity. Next, $Bi_{25}Fe_2O_{39}$ or $Bi_{25}FeO_{40}$ in some samples is paramagnetic or only ferromagnetic at low temperature. Finally, $Bi_2Fe_4O_9$ is antiferromagnetic with $T_N \sim 260$ K [29]. Based on above considerations, the ferromagnetic ordering in this system can be considered as intrinsic and ascribed to the collapse of the spiral spin structure by a structural distortion. Moreover, it can further certify that the XRD patterns are pure.

4 Conclusions

In summary, the $0.6BiFeO_3$–$0.4(Bi_{0.5}Na_{0.5})_{(1-x)}Ba_xTiO_3$ ($x = 0$, 0.2, 0.3, 0.4, 0.5) solid-solution ceramics were fabricated by a sol–gel method. All the samples are pure phase. The properties of ferroelectric, dielectric and magnetic have been investigated. Samples with different doping contents of Ba present corresponding ferroelectric and magnetic properties at room temperature. The peak position of dielectric constant shifts toward to lower temperature, and the dielectric diffuse degree increases monotonically with the increasing of x. The maximum values of P_r and M_r occur at $x = 0.4$ simultaneously. These results prove the coexistence of magnetism and ferroelectricity at room temperature. The multiferroic properties are well enhanced with different doping contents of Ba ions.

Acknowledgments This work was supported by the National Natural Science Foundation of China (Grant Nos. 11174092 and 11474111). We would like to thank the staff of Analysis Center of HUST for their assistance in various measurements.

References

1. Spaldin NA, Fiebig M (2005) The renaissance of magnetoelectric multiferroics. Science 309:391–392

2. Nan CW, Bichurin MI, Dong SX, Viehland D, Srinivasan G (2008) Multiferroic magnetoelectric composites: historical perspective, status, and future directions. J Appl Phys 103:031101
3. Eerenstein W, Mathur ND, Scott JF (2006) Multiferroic and magnetoelectric materials. Nature 442:759–765
4. Chaudhuri AR, Krupanidhi SB (2010) Investigation of true remnant polarization response in heterostructured artificial biferroics. Solid State Commun 150:660–662
5. Hill NA (2000) Why are there so few magnetic ferroelectric. J Phys Chem B 104:6694–6709
6. Kumar N, Panwar N, Gahtori B, Singh N, Kishan H, Awana VPS (2010) Structural, dielectric and magnetic properties of Pr substituted $Bi_{1-x}Pr_xFeO_3$. J Alloy Compd 501:29–32
7. Feridoon A, Robert F, Michael T, Robert C, Floriana T, David C (2010) Microstructure and properties of Co-, Ni-, Zn-, Nb- and W-modified multiferroic $BiFeO_3$ ceramics. J Eur Ceram Soc 30:727–736
8. Kumar MM, Palkar VR, Srinivas K, Suryanarayana SV (2000) Ferroelectricity in a pure $BiFeO_3$ ceramic. Appl Phys Lett 76:2764
9. Ghosh AK, Dwivedi GD, Chatterjee B, Rana B, Barman A, Chatterjee S, Yang HD (2013) Role of codoping on multiferroic properties at room temperature in $BiFeO_3$ ceramic. Solid State Commun 166:22–26
10. Sakata K, Takenaka T, Naitou Y (1992) Phase relations, dielectric and piezoelectric properties of ceramics in the system $(Bi_{0.5}Na_{0.5})TiO_3$–$PbTiO_3$. Ferroelectrics 131:219–226
11. Huo SX, Yuan SL, Qiu Y, Ma ZZ, Wang CH (2012) Crystal structure and multiferroic properties of $BiFeO_3$–$Na_{0.5}K_{0.5}NbO_3$ solid solution ceramics prepared by Pechini method. Mater Lett 68:8–10
12. Ma ZZ, Tian ZM, Li JQ, Wang CH, Huo SX, Duan HN, Yuan SL (2011) Enhanced polarization and magnetization in multiferroic $(1-x)BiFeO_3$–$xSrTiO_3$ solid solution. Solid State Sci 13: 2196–2200
13. Dorcet V, Trolliard G, Boullay P (2008) Reinvestigation of phase transitions in $Na_{0.5}Bi_{0.5}TiO_3$ by TEM. Part 1: first order rhombohedral to orthorhombic phase transition. Chem Mater 20: 5061–5073
14. Wu JG, Kang GQ, Liu HJ, Wang J (2009) Ferromagnetic, ferroelectric and fatigue behavior of (111)-oriented $BiFeO_3$/$(Bi_{0.5}Na_{0.5})TiO_3$ lead free bilayered thin films. Appl Phys Lett 94: 172906
15. Singh A, Pandey V, Kotnala RK, Pandey D (2008) Direct evidence for multiferroic magnetoelectric coupling in $0.9BiFeO_3$–$0.1BaTiO_3$. Phys Rev Lett 101:247602
16. Tian ZM, Zhang YS, Yuan SL, Wu MS, Wang CH, Ma ZZ, Huo SX, Duan HN (2012) Enhanced multiferroic properties and tunable magnetic behavior in multiferroic $BiFeO_3$–$Bi_{0.5}Na_{0.5}TiO_3$ solid solutions. Mater Sci Eng, B 177:74–78
17. Lei ZW, Huang Y, Liu M, Ge W, Ling YH, Peng R, Mab XY, Chen XB, Lu YL (2014) Ferroelectric and ferromagnetic properties of $Bi_{7-x}La_xFe_{1.5}Co_{1.5}Ti_3O_{21}$ ceramics prepared by the hot-press method. J Alloy Compd 600:168–171
18. Kumar M, Shankar S, Kotnala RK, Parkash O (2013) Evidences of magneto-electric coupling in BFO-BT solid solutions. J Alloy Compd 577:222–227
19. Qin HB, Zhang HL, Zhang BP, Xu LH (2011) Hydrothermal synthesis of perovskite $BiFeO_3$–$BaTiO_3$ crystallites. J Am Ceram Soc 94:3671–3674
20. Kim JW, Do D, Kim SS (2012) Enhanced electrical properties of rare-earth-substituted $(Bi_{0.9}RE_{0.1})(Fe_{0.975}Cr_{0.025})O_3$ (RE = Nd, Gd, Eu) thin films. J Korean Phys Soc 61:1404–1408
21. Leontsev SO, Eitel RE (2009) Dielectric and piezoelectric properties in Mn-modified $(1-x)BiFeO_3$–$xBaTiO_3$ ceramics. J Am Ceram Soc 92:2957–2961
22. Wu MS, Huang ZB, Han CX, Yuan SL, Lu CL, Xia SC (2012) Enhanced multiferroic properties of $BiFeO_3$ ceramics by Ba and high-valence Nb co-doping. Solid State Commun 152:2142–2146
23. Katlakunta S, Raju P, Meena SS, Srinath S, Sandhya R, Kuruva P, Murthy SR (2014) Multiferroic properties of microwave sintered $BaTiO_3$–$SrFe_{12}O_{19}$ composites. Phys B 448:323–326
24. Merz WJ (1949) The electric and optical behavior of $BaTiO_3$ single-domain crystals. Phys Rev 76:1221–1225
25. Smolensky GA, Isupov VA, Agranovskaya AI, Krainik NN (1961) New ferroelectrics of complex composition. Sov Phys Solid State 2:2651–2654
26. Palkar VR, Kundaliya DC, Malik SK, Bhattacharya S (2004) Magnetoelectricity at room temperature in the $Bi_{0.9-x}Tb_xLa_{0.1}FeO_3$. Phys Rev B 69:212102
27. Meera R, Yadav KL (2013) Structural, dielectric and ferroelectric properties of $Ba_{1-x}(Bi_{0.5}Na_{0.5})_xTiO_3$. Ceram Int 39:3627–3633
28. Uchino K, Nomura S (1982) Critical exponents of the dielectric constants in diffused-phase-transition crystals. Ferroelectrics 44:55–61
29. Tian ZM, Yuan SL, Wang XL, Zheng XF, Yin SY, Wang CH, Liu L (2009) Size effect on magnetic and ferroelectric properties in $Bi_2Fe_4O_9$ multiferroic ceramics. J Appl Phys 106:103912